A time-of-flight system for the external target facility *

ZHANG Xue-Heng(章学恒)[1;1)] YU Yu-Hong(余玉洪)[1] SUN Zhi-Yu(孙志宇)[1] MAO Rui-Shi(毛瑞士)[1]
WANG Shi-Tao(王世陶)[1] ZHOU Yong(周勇)[1,2] YAN Duo(闫铎)[1,2] LIU Long-Xiang(刘龙翔)[1,2]

[1] Institute of Modern Physics, Chinese Academy of Sciences, Lanzhou 730000, China
[2] Graduate University of Chinese Academy of Sciences, Beijing 100049, China

Abstract: A time-of-flight system with a plastic scintillator coupled to photomultipliers is developed for the external target facility (ETF). This system can satisfy the requirement of an ultrahigh vacuum ($\sim 10^{-9}$ mbar), a high counting rate ($\sim 10^6$ particles per second) and a magnetic field environment. In the beam test experiment, a total time resolution of 580 ps FWHM was obtained for the whole system, and nuclei with a mass of up to 80 could be identified using this system.

Key words: ETF, RIBLL2, TOF time resolution

PACS: 29.40.Mc **DOI:** 10.1088/1674-1137/37/5/056002

1 Introduction

An external target facility (ETF) is constructed downstream of the second radioactive ion beam line (RIBLL2) in the Heavy Ion Research Facility in Lanzhou (HIRFL) [1, 2]. It consists of a series of sub-detector systems, such as the γ ball [3], TOF wall [4], neutron wall [5], and MWPCs [6]. Using beams that can accelerate nuclei up to ^{238}U with a kinetic energy of several hundreds of MeV to GeV using the main Cooling Storage Ring (CSRm) [2], research on the structure of exotic nuclei and the equation of state of dense nuclear matter can be carried out at the ETF.

Like the FRS (GSI FRagment Separator), which delivers radioactive ion beams (RIBs) to the ALADIN-LAND setup for decay and reaction studies at GSI [7, 8], the first half of RIBLL2 can be used to produce and separate the interested RIBs for ETF. The RIBs can be identified by combining the time-of-flight (TOF), the energy deposit ΔE and the magnetic rigidity $B\rho$, which is widely used by all projectile fragmentation type separators. Therefore, a TOF system, which provides experimental trigger and particle identification, should be developed for the ETF. This system should satisfy the following stringent requirements: (1) the start detector should have a large area ($\sim$100 mm$\times$100 mm), be used in the ultrahigh vacuum ($\sim 10^{-9}$ mb), and should withstand a high counting rate ($\sim 10^6$ particles per second); (2) the stop detector should be operated in the magnetic field environment (<0.01 T); and (3) the TOF system should have a good mass resolution power (up to 60).

In this paper, we would like to report the design of this TOF system. The measurements results will also be presented.

2 The design of the TOF system

The layout of the first half of the RIBLL2 and ETF is shown in Fig. 1. The primary beam from CSRm hits a target at the F0 cave. The RIBs produced by projectile fragmentation are separated and purified by the combined $B\rho$-ΔE-$B\rho$ method [9], and then delivered to the ETF for experimental studies. Particle identification is implemented before the second target. To obtain a good mass resolution, the flight path should be as long as possible, so we place the start and stop detectors at the F1 cave and upstream of the second target, respectively. The total length of the flight path is about 26 m.

2.1 The start detector

The start detector is designed based on a plastic scintillator from the manufacturer Eljen (EJ200) [10]. Hamamatsu R7111 photomultipliers [11] are used to read out the signals from both ends of the scintillator.

According to the beam optics calculations [12], the beam spots have maximum position dispersion at the F1 cave. The beam size is about 100 mm$\times$100 mm when the slits are fully opened. The plastic scintillator, which has the feature of no size restrictions, can be easily made into a large area detector to meet the size requirement.

Received 26 June 2012
* Supported by National Natural Science Foundation of China (11205210)
1) E-mail: zhxh@impcas.ac.cn

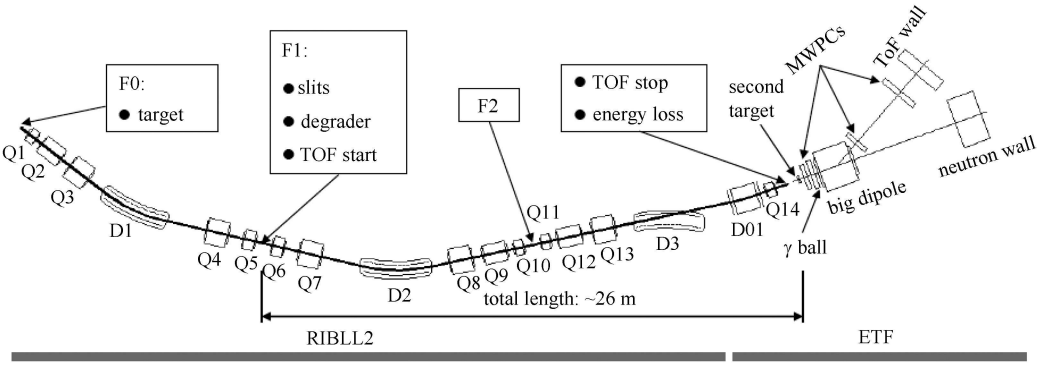

Fig. 1. Top view of the first half of the RIBLL2 and ETF.

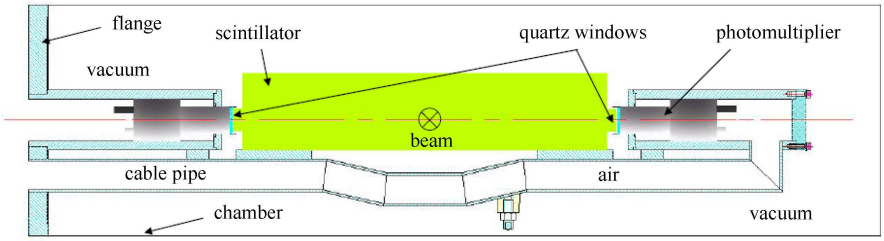

Fig. 2. (color online) Schematic layout of the start detector.

The start detector will be used in ultrahigh vacuum (at a pressure of $\sim 10^{-9}$ mb). This calls for very low outgassing materials in the mechanical support, optical coupling, a voltage divider and cables. A specific stainless steel frame has been designed and its schematic layout is shown in Fig. 2. The whole frame is fixed on a flange connected with the F1 chamber. The scintillator is placed in the center of the beam line, and photomultipliers are fixed in the cylinders at both ends of the scintillator. Two 3 mm thick circular quartz windows are welded at one end of two cylinders to isolate the air and to transmit photons from the scintillator to the photomultipliers. The couplings via optical silicon pads and a vacuum are chosen between the photomultipliers and quartz windows, and between the quartz windows and scintillator, respectively. With this frame all the materials except the scintillator are placed in the atmosphere to ensure that the start detector is less affected by the outgassing rate.

To ensure the air tightness of the welded interfaces, the quartz windows can only be processed into a circle with a maximum diameter of 35 mm due to the constraints of the machining technology. The light collection efficiency will be influenced by the difference in sizes between the scintillator and the quartz windows. The light collection efficiency of two prototypes has been simulated with GEANT4 [13]. Prototype I, shown in Fig. 3(a), consists of a scintillator of dimension 100 mm×100 mm×3 mm and two vacuum-coupled light guides. Prototype Ⅱ, shown in Fig. 3(b), is a monoblock scintillator without four corners. The thickness of Propotype Ⅱ is 3 mm, and the widths of the cut and uncut parts are 30 mm and 100 mm, respectively. The total length of the two prototypes, which is equal to the distance of two quartz windows, is 500 mm. In the simulation both the scintillator and light guides are covered by thin aluminum foil, the refraction of the scintillator and light guide is 1.58, and the vacuum refraction is 1.0. A primary beam of 500 MeV/u ^{12}C with a spot size of 80 mm in diameter hits the center of the scintillator. The photons will be produced by the scintillation process due to the electromagnetic energy loss of ^{12}C. The light collection efficiency is calculated by the ratio between the photons transmitted to the end (N_1) and the total photons (N_0). Fig. 3(c) shows the light collection efficiency as a function of the length of the vacuum layers between the scintillator and light guides for Prototype Ⅰ, and Fig. 3(d) shows the light collection efficiency change with the length of the cut corners for Prototype Ⅱ. It can be seen that the light collection efficiency slightly increases with a decrease in the length of the cut corners, and the value is similar to the efficiency at the vacuum length of 1 mm. Considering the accuracy of machining, Prototype Ⅱ is finally adopted with a cut corner length of 6 mm. The scintillator is covered by one layer of 6 μm thick aluminum foil, and the length between the scintillator and the quartz window is about 1 mm.

When the start detector is running at high rate, the

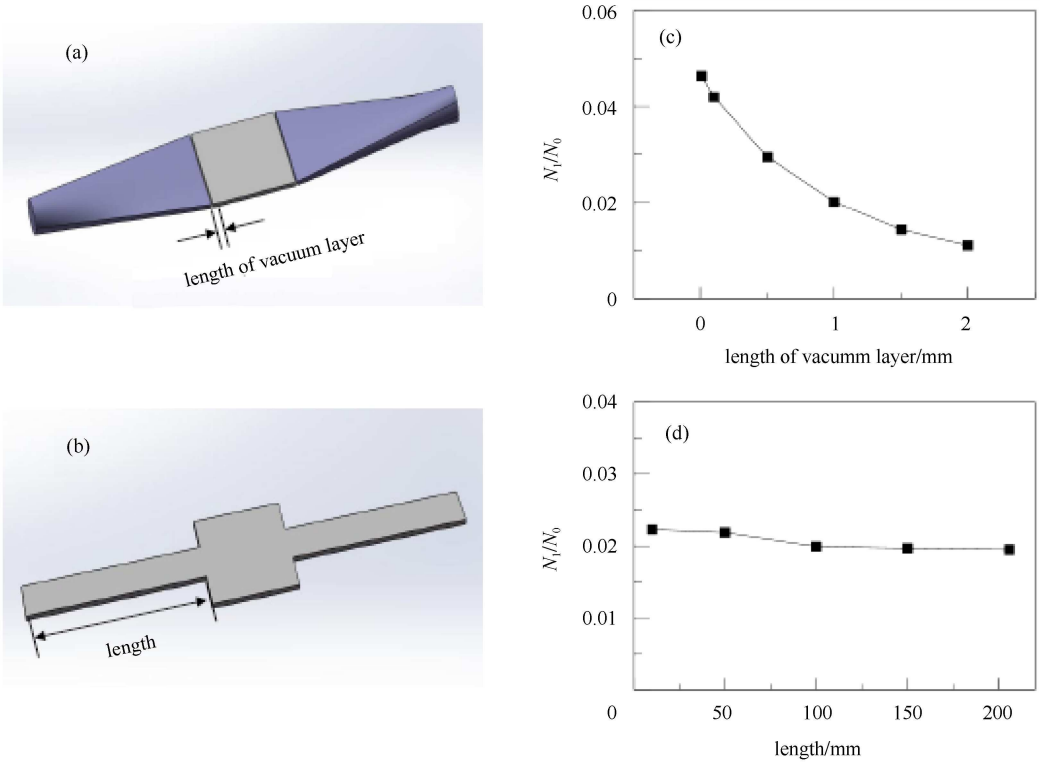

Fig. 3. (color online) Light collection efficiency simulated with GEANT4. (a) and (b) are a schematic diagram of prototypes Ⅰ and Ⅱ, (c) is the efficiency as a function of the length of the vacuum layer of Prototype Ⅰ, and (d) shows the efficiency as a function of the length of cut corners of Prototype Ⅱ.

anode current of the photomultipliers increases dramatically, and the non-linearity effect appears in such a way that the voltage drop in the last amplification stages becomes significant and causes gain instability due to insufficient bleeder current supply [14]. To keep the photomultiplier gain stable against the incoming particle flux (up to $\sim 10^6$ particles per second), three types of voltage dividers are designed, as shown in Fig. 4(a), (b) and (c), respectively. Type Ⅰ is a traditional voltage divider. Type Ⅱ is an improved voltage divider with a large-scale regulated power supply network, and Type Ⅲ adopts the additional power supplies at the last three dynodes based on Type Ⅱ. The divider ratios of the three types of voltage dividers have been adjusted to obtain good gain [15]. In order to evaluate the rate capability of our prototypes, a test was performed. A green LED (light emitting diode) source [16], which was driven by the square signal with an amplitude of 5 V, width of 40 ns, leading edge of 13 ns and trailing edge of 12.1 ns, was used to simulate an increasing particle rate. Using an optical fiber, the light output was delivered to the center of the R7111 photomultiplier with a high voltage of −900 V. The amplitude of the photomultiplier output signal directly measured by an oscilloscope was studied as a function of the LED frequency. The results are shown in Fig. 4(d). When the frequency is increased, the amplitude remains constant up to a maximum value $\sim 10^4$ Hz for the three voltage dividers, and then the amplitude increases first and then reduces. The reason for the amplitude increase can be explained as the overlap of the LED electroluminescence. From Fig. 4(d) we can see that the Type Ⅲ voltage divider can still keep the photomultiplier gain stable at about 10^6 Hz. So the Type Ⅲ voltage divider is used in our detector.

The start detector has been tested with a ^{60}Co gamma ray source, and the coincidence signals of both ends of the detector measured with an oscilloscope are shown in Fig. 5(a), (b) and (c) when the source was put at the center, left and right positions of the scintillator, respectively. It can be seen that the time and amplitudes of two coincidence signals are similar when the source is put at the center. When the source is put at one side, the signal from this side is earlier and bigger than the one from the other side.

2.2 The stop detector

The stop detector will be placed near the second target. This is a focus point, and the beam size is smaller than the one on the start detector. So a 50 mm× 50 mm×1 mm BC408 scintillator sheet [17] coupled to two photomultipliers at both ends with optical glue is

used for the stop detector. Since the position of the stop detector is near the big dipole of the ETF, the leakage magnetic flux has a serious influence on the signal amplitude of the photomultiplier. Therefore, the R7111 photomultipliers have been replaced by fine mesh R7761 photomultipliers [11], which can be operated even in strong magnetic fields over 1.0 T [18, 19]. A large-scale regulated power supply network and additional power supplies for the last three dynodes were also applied for the R7761 voltage divider.

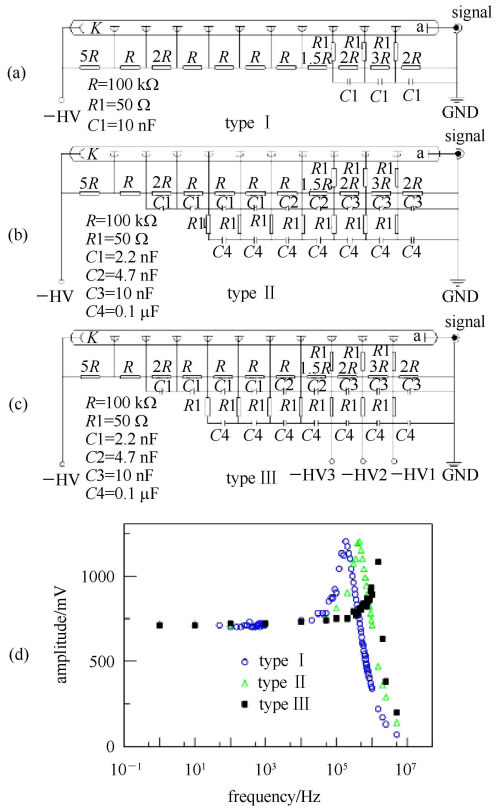

Fig. 4. (color online) Three types of voltage dividers for the R7111 photomultiplier shown in (a), (b) and (c), respectively. The signal amplitudes as a function of LED frequency are shown in (d).

3 The beam test

The TOF system was installed and used experimentally. A primary beam of 400 MeV/u ^{12}C was extracted from CSRm and implanted into a 15.1 mm thick ^{9}Be target at the F0 cave of RIBLL2. The fragmentation products were separated and identified by the first half of RIBLL2. In the experiment, the magnetic rigidity was set to 4.57 Tm, which was calculated with ^{9}C nuclei. The slits located at the F1 cave were opened at ±10 mm, and the degrader was not used.

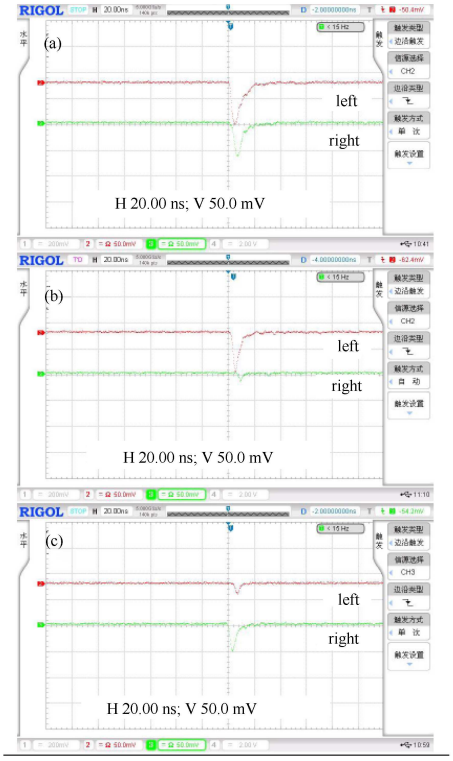

Fig. 5. (color online) Coincidence signals of the start detector measured with a ^{60}Co gamma ray source. (a), (b) and (c) show the results when the source was put at the center, left and right of the scintillator, respectively.

A typical ΔE-TOF spectrum is shown in Fig. 6(a). The energy loss was measured by a 140 μm thick 45 mm×45 mm silicon detector. Fig. 6(b) shows a TOF spectrum only for the ^{9}C nuclei chosen in Fig. 6(a). The root-mean-square width of this distribution is determined to be 2.92. Considering the TDC channel width of 84.7 ps [20], a time resolution of 580 ps (full width at half maximum, FWHM) was obtained for the whole system. This value includes all the factors that cause time dispersion, such as fragment energy dispersion and electronics.

The mass resolution power of the TOF system is given by the following relationships [21],

$$R=\frac{A}{\Delta A}=\frac{T}{\Delta T}, \tag{1}$$

where A and T are the mass and time-of-flight of the nuclei, and ΔA and ΔT are the widths of the mass peak and time-of-flight peak, respectively. With the RIBLL2 maximum magnetic rigidity of 10.64 Tm [2], the highest velocity $\beta_{\max}$ is about 0.915 for the ion with the mass to charge ratio of 1.5. From Eq. (1) we obtain the mass resolution power $R\leqslant 160$, and nuclei with a mass of up to 80 could be identified using this TOF system.

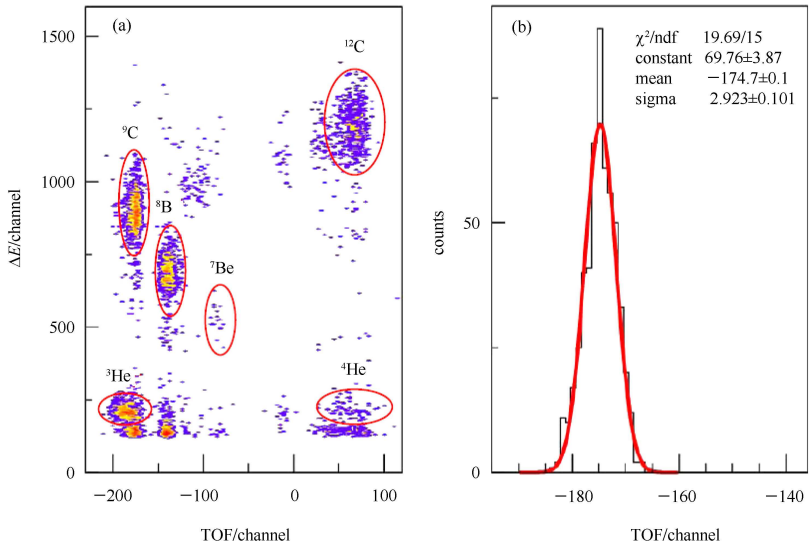

Fig. 6. (color online) The particle identification spectrum for ^{12}C+^{9}Be at 400 MeV/u (a). The TOF spectrum of ^{9}C is shown in (b), and the red line denotes the fitting results with Gaussian function.

4 Summary

In this paper, a TOF system with a plastic scintillator coupled to photomultipliers was developed for the ETF. The start and stop detectors are installed at the F1 cave of RIBLL2 and upstream of the second target, respectively. The distance of this TOF system is about 26 m. The special design of the frame makes the start detector work in ultrahigh vacuum. To obtain high light collection efficiency, a monoblock scintillator without four corners was adopted by the simulations. Photomultipliers for a high magnetic environment were used in the stop detector to resist the leakage magnetic flux of the big dipole. The voltage dividers for both detectors were designed as a large-scale regulated power supply network with additional power supplies at the last three dynodes, which makes the photomultiplier gain stable at incoming particle flux up to $\sim 10^6$ particles per second. This TOF system was used experimentally and a total time resolution of 580 ps FWHM was obtained. Nuclei with a mass of up to 80 could be identified using this system.

The authors gratefully acknowledge Meng Jun-Hou Shen-Jun and Zhao Yu-Gang for their support on the vacuum technique.

References

1 XIA J W, WANG Y F, RAO Y N et al. HIRFL Status and HIRFL-CSR Project in Lanzhou. Proceeding of the First Asian Paticle Accelerators Conference. Japan: KEK, 1998. 342
2 XIA J W, ZHAN W L, WEI B W et al. Nucl. Instum. Methods. A, 2002, **488**: 11
3 YEI K. Design and Simulation Studies of CsI(TI) Scintillator Detector Array for External Target Facility at HIRFL-CSR (Ph.D.Thesis). Lanzhou: Instumitute of Modern Physics, CAS, 2010 (in Chinese)
4 YU Y H. Development and Construction of Fast Plastic Scintillator Detector Array for External Target Experiment at CSRm (Ph.D.Thesis). Lanzhou: Instumitute of Modern Physics, CAS, 2009 (in Chinese)
5 XU H G. Design and Construction of Neutron Wall for External Target Experiment at CSRm of HIRFL-CSR (Ph.D.Thesis). Lanzhou: Instumitute of Modern Physics, CAS, 2006 (in Chinese)
6 LU C G. Study of RIBLL2 External Target Gaseous Track Detector (Ph.D.Thesis). Lanzhou: Instumitute of Modern Physics, CAS, 2011 (in Chinese)
7 Blaich T H, Elze T W, Emling H et al. Nucl. Instrum. Methods A, 1992, **314**: 136
8 Geissel H, Armbruster P, Behr K H et al. Nucl. Instrum. Methods B, 1992, **70**: 286
9 Schmidt K H, Hanelt E et al. Nucl. Instrum. Methods A, 1987, **260**: 287
10 http://www.eljentechnology.com/images/stories/Data_Sheets/Plastic_Scintillators/EJ200%20data%20sheet.pdf
11 http://www.hamamastu.com
12 SONG M T, YANG X D, XIA J W et al. HEP & NP, 2001, **25**(5): 443 (in Chinese)
13 http://geant4.cern.ch
14 LEO W R. Techniques for Nuclear and Particle Physics Experiments. 2nd Revised Edition. Berlin: Springer, 1994
15 DING X L, WANG J C, QI H R et al. Nuclear Electronics & Detection Technology. 2005, **25**(4): 392
16 http://www.z-light.com.cn/Upload/PDF/20110804135342887552.pdf
17 http://www.phys.ufl.edu/courses/phy4803L/group_I/muon/bicron_bc400-416.pdf
18 Lijima T, Amami M, Adachi I et al. Nucl. Instrum. Methods A, 1997, **387**: 64
19 Bonesini M, Strati F, Baccaglion et al. Nucl. Instrum. Methods A, 2006, **567**: 200
20 http://www.caen.it/csite/CaenProd.jsp?parent=11&idmod=35#
21 SUN Z Y, ZHAN W L, GUO Z Y et al. Nucl. Instrum. Methods A, 2003, **503**: 496